JOURNAL OF MOLECULAR SPECTROSCOPY 157, 55–67 (1993)

The Rotational Spectrum of OH in the $v = 0$–3 Levels of Its Ground State

THOMAS D. VARBERG[1] AND KENNETH M. EVENSON

Time and Frequency Division, National Institute of Standards and Technology, 325 Broadway, Boulder, Colorado 80303

Rotational and fine structure transitions have been observed between low rotational levels in the $v = 0$–3 levels of the OH $X^2\Pi$ state by tunable far-infrared spectroscopy. The rotational and fine structure constants of the ground state have been refined by least-squares fitting to the observed data in combination with far-infrared and microwave measurements by other authors. Pressure-induced frequency shifts with helium as a buffer gas are also reported for some of the $v = 0$ transitions.

1. INTRODUCTION

Spectroscopic information regarding the hydroxyl radical (OH) is important for investigations on a wide variety of physical and chemical problems. The OH radical is one of the most abundant molecular free radicals in the atmosphere (*1, 2*) and is important in combustion processes (*3*). OH is also abundant in the interstellar medium, having been identified as early as 1963 by its microwave masing transitions (*4*) and later detected at wavelengths in the far infrared (*5*). Recent theoretical work has focused on calculating the proton hyperfine structure in OH (*6–8*) and the ^{17}O hyperfine structure in ^{17}OH (*8*). For these and other reasons, the spectroscopic information on OH is particularly comprehensive. The available spectroscopic data involving the $X^2\Pi$ and $A^2\Sigma^+$ states of OH were critically reviewed by Coxon in 1980 (*9*). In this work Coxon performed a global least-squares fit to microwave, infrared and optical transitions, thereby determining accurate values of the molecular parameters for the X ($v \leq 5$) and A ($v \leq 3$) states.

In this paper we report far-infrared (FIR) absorption spectra of OH in the first four vibrational levels of its ground state recorded using the technique of tunable far-infrared (TuFIR) spectroscopy. The work on the $v = 0$ level of the $X^2\Pi$ state duplicates a previous TuFIR experiment by Brown *et al.* (*10*) in this laboratory, but with a tenfold increase in accuracy. Far-infrared, pure rotational transitions within the $v = 1$, 2, and 3 levels are reported here. We observed transitions between the lowest rotational levels in both spin components of the ground state for $v \leq 3$, as well as fine structure transitions within the $v = 0$ and 1 levels (see Fig. 1). In combination with data reported by other authors, the present measurements have allowed us to refine the rotational, spin–orbit, and spin–rotation parameters of the $v = 0$–3 levels, as well as the lambda-doubling parameters of the $v = 3$ level.

[1] Present address: Physical Chemistry Laboratory, Oxford University, South Parks Road, Oxford OX1 3QZ, United Kingdom; permanent address: Department of Chemistry, Macalester College, St. Paul, MN 55105.

0022-2852/93 $5.00

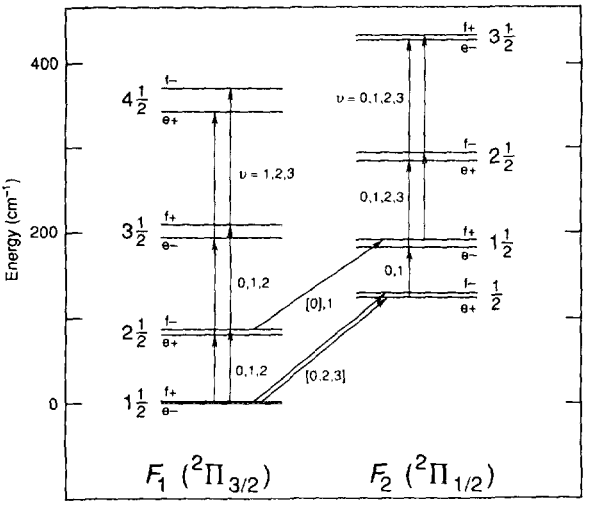

FIG. 1. Energy level diagram of the OH ground state, indicating the positions of the $v = 0$ rotational levels (the relative positions of the rotational levels in the $v = 1$, 2, and 3 levels are similar). The parity components are labeled both by their e/f symmetries and by their absolute parities; the lambda-doubling has been magnified by a factor of 35 for clarity. Arrows and vibrational numbers mark the observed far-infrared transitions, with brackets signifying transitions observed by other authors.

2. EXPERIMENTAL DETAILS

The TuFIR experimental technique has been described in detail elsewhere (*11, 12*). Briefly, far-infrared radiation is generated by mixing the mid-infrared radiation from two frequency-stabilized CO_2 lasers (with frequencies ν_I and ν_{II}) on a metal–insulator–metal (MIM) diode. In second order the FIR difference frequency $|\nu_I - \nu_{II}|$ is tuned by varying the frequency of one of the CO_2 lasers over its gain curve. Greater tunability (but less FIR power) is obtained in third order by mixing in radiation from a microwave synthesizer (with frequency ν_μ), generating two tunable frequencies $|\nu_I - \nu_{II}| \pm \nu_\mu$. With a choice of about 5000 pairs of $^{12}C^{16}O_2$ laser lines (*13*), all FIR frequencies up to 5 THz can be generated by third-order mixing.

Two sources for generating OH were used in these experiments. The first source was a DC hollow cathode discharge through water and argon. The discharge cell was a 0.6-m long, 14-mm inner diameter copper pipe, with 75-μm polypropylene windows at each end. Two wire anodes entered the tube 15 cm from each end. The typical potential drop across the tube was 350 V, producing a current of 100 mA. Argon and H_2O in a ratio of ~50:1 were introduced into the cell near the windows; the total pressure was ~100 Pa (0.75 Torr). This source produced ground state OH in its $v = 0$, 1, 2, and 3 levels in an approximate ratio of 20:10:5:1 (see Fig. 2). The weak $v = 3$ signals discouraged us from attempting to measure $v = 4$ transitions.

As we discuss in detail in the next section, the hollow cathode discharge source produced measurable Stark shifts of the OH transitions. Therefore, we developed a second molecular source which employed an external microwave discharge. In this source, helium was bubbled through water and passed through a 50-W, 2450-MHz microwave discharge in a quartz tube. The microwave cavity was located 12 cm above the center of a 2.5-m long, 20-mm inner diameter Teflon cell, with 75-μm polypropylene windows at each end. A Teflon cell and fittings were used in order to minimize

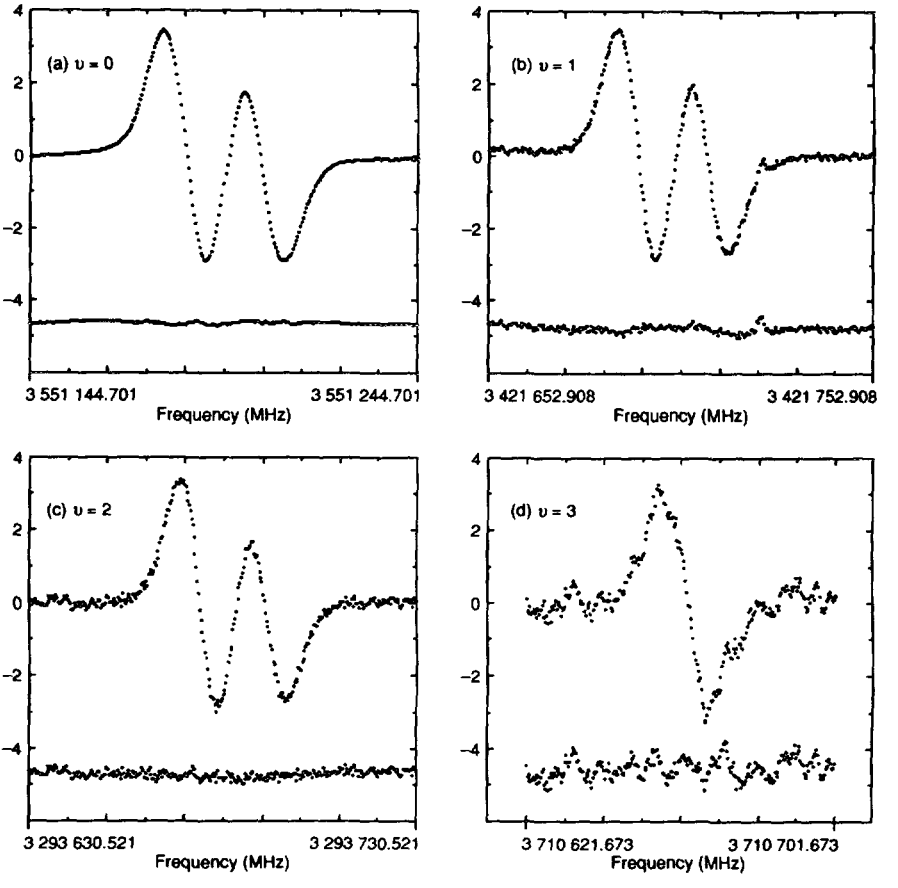

FIG. 2. Experimental spectra of pure rotational transitions within the $v = 0$–3 levels of the OH ground state. The upper traces are the experimental data and the lower traces are the residuals obtained from least-squares fits to the observed lineshapes. Spectra (a)–(c) are of the F_1–F_1 ($J = 3\frac{1}{2}^+$–$2\frac{1}{2}^-$) transition in the $v = 0$–2 levels, for which the proton hyperfine splitting is nearly resolved. Spectrum (d) is of the $v = 3$, F_2–F_2 ($J = 3\frac{1}{2}^+$–$2\frac{1}{2}^-$) transition, for which the two strong hyperfine components are completely blended.

loss of OH at the cell walls. The signals of $v = 0$ transitions in this source were comparable in strength to those in the hollow cathode discharge source, but $v = 1$ transitions were far weaker. OH molecules were detected at distances between 0.1 and 1.4 m from the microwave discharge, resulting in a vibrational distribution which was colder than that produced in the electric discharge source.

A length scrambler was inserted in the FIR radiation path in order to eliminate standing waves (*14*); this flattens the spectrometer baseline and improves our ability to measure the transition line centers. The OH spectrum was recorded as a first derivative by frequency-modulating one of the two CO_2 lasers at 1 kHz and detecting the absorption signal with a lock-in amplifier. A photoconductor was used for all transitions except the $v = 1$, F_2–F_2 ($J = 1\frac{1}{2}^-$–$\frac{1}{2}^+$) transition at 1.76 THz, for which a Ge bolometer was used. We used a 300-msec time constant on the lock-in amplifier and scanned each spectral line twice—once in each direction of the FIR frequency—and collected and averaged these two scans by computer. On weaker lines, additional pairs of scans were collected and averaged in order to improve the signal-to-noise

ratio. A typical 100-MHz scan was recorded in 3 min in each direction, collecting about six data points per MHz.

The lineshapes of the OH spectra were fitted by least squares using a computer program developed by Chance *et al.* (*15*). We recorded spectra of $\Delta J = \pm 1$ transitions only; consequently, each transition contained three ^{1}H ($I = \frac{1}{2}$) hyperfine components: two strong $\Delta F = \pm 1$ components and a weak $\Delta F = 0$ component. Usually these hyperfine components were partially or completely blended. In fitting each rotational line, we fixed both the relative intensities of the three components and their frequency splittings. The relative intensities were calculated from the usual expression (*16*). The frequency splittings of $v = 1$, 2, and 3 transitions were taken from Coxon's work (*9*), which is based on higher resolution microwave measurements of lambda-doubling transitions. The $v = 0$ hyperfine splittings were taken from the laser magnetic resonance (LMR) work of Brown *et al.* (*17*). Typically, five parameters were varied in fitting a spectral lineshape: the transition frequency and intensity of the strongest hyperfine component, the Gaussian and Lorentzian linewidths of the three components, and the spectrometer baseline. However, linear, quadratic, or cubic terms were occasionally added to the baseline and varied to correct for residual standing waves.

3. DATA ANALYSIS

(A) Stark Shifts in the DC Electric Discharge Source

In Fig. 2 we display spectra recorded using the hollow cathode discharge source. A preliminary least-squares fit of the $v = 1$ transitions recorded with this source revealed that the measured transition frequencies were not fitting within the estimated measurement errors. Systematic residuals in the fit suggested that the DC electric discharge was producing small but measurable Stark shifts of the rotational levels.

Stark shifts in a degenerate ($\Lambda \neq 0$) state are caused by electric field-induced mixing of the two parity components of a rotational level. The Stark matrix elements have been given by Gordy and Cook (*18*),

$$\langle {}^{2S+1}\Lambda;\ J^{\pm} M\Omega | H_{\text{Stark}} | {}^{2S+1}\Lambda;\ J^{\mp} M'\Omega' \rangle = \frac{-\mu \mathcal{E} M\Omega}{J(J+1)} \delta_{MM'} \delta_{\Omega\Omega'}, \tag{1}$$

where μ is the molecular dipole moment, $\mathcal{E}$ is the applied electric field and the $\pm$ signs designate the parity. Using second-order perturbation theory, we can estimate the energy level shifts caused by the Stark effect as

$$\Delta E = \frac{|\langle {}^{2S+1}\Lambda;\ J^{\pm} M\Omega | H_{\text{Stark}} | {}^{2S+1}\Lambda;\ J^{\mp} M'\Omega' \rangle|^2}{E^0_{JM\Omega} - E^0_{JM'\Omega'}}, \tag{2}$$

where E^0 designates the unperturbed energy of the rotational level.

Equations (1) and (2) predict certain trends in the Stark shifts of a $^2\Pi$ molecule: (1) The energy shifts are equal and opposite in the two parity components of a rotational level, (2) the shifts are inversely proportional to the size of the lambda-doubling, and (3) the shifts decrease rapidly as the molecular rotation increases because of the J-dependence of the matrix elements.

To investigate these Stark shifts, we measured $v = 0$ transitions in both the DC electric discharge source and the external microwave discharge source for comparison. The observed Stark shifts of the $v = 0$ rotational transitions are not accurately predicted by Eqs. (1) and (2). For this reason, we decided to use the $v = 0$ Stark shifts to calibrate the $v = 1$–3 frequencies measured in the DC discharge source in the following manner:

we measured the Stark shift of each $v = 0$ transition for various values of the applied voltage and then interpolated Stark shifts for the $v = 1$–3 transitions for the specific voltage used. Thus we are assuming that the Stark shifts of the $v = 0$ transitions are identical to those of the corresponding $v = 1$–3 transitions. Since the lambda-doubling of a particular rotational level in the $v = 1$, 2, and 3 levels is similar in size (within 20%) to that in the corresponding $v = 0$ level, we think that this procedure is accurate. The largest $v = 0$ Stark shift we observed was 1.1 MHz. We estimate that the frequency uncertainty of a $v = 1$–3 transition calibrated in this way is 200 kHz.

(B) Pressure Shifts in the External Microwave Discharge Source

We observed pressure shifts of the $v = 0$ transitions recorded with the external microwave discharge source. To correct for these shifts, we typically recorded the spectrum of a particular rotational transition at five different pressures in the pressure region between 130 and 1300 Pa (1 and 10 Torr); below 130 Pa the signal intensities were too weak for accurate measurements. By the method of weighted least squares we fit a line to the measured frequencies as a function of pressure. The pressure shifting coefficient is given by the slope of the fitted line and the transition frequency at zero pressure is given by the y-intercept. These are listed in Table I for the $v = 0$ transitions we studied. Figure 3 displays the experimental and fitted pressure shifts for two of the $v = 0$ transitions. These results are in contrast to an earlier TuFIR study of the pressure broadening of OH (*15*), in which the authors did not observe statistically significant OH pressure shifts with He (or H_2, N_2, or O_2) as the buffer gas.

(C) The Effective Hamiltonian

We fitted the OH $X^2\Pi$ transitions with an effective Hamiltonian written in a Hund's case (a) basis using an $\mathbf{N}^2$ formalism (*19*). In this formalism, the rotational operator is written as $B\mathbf{N}^2 = B(\mathbf{J} - \mathbf{S})^2$. Many authors, in particular Coxon in his global fit of the OH molecule (*9*), use an $\mathbf{R}^2$ formalism, where the rotational operator is written

TABLE I

Pressure Shifts of OH $X^2\Pi$ ($v = 0$) Far-Infrared Transitions with Helium as Buffer Gas

Transition			Pressure Shift[b]	
F_i'–F_i''	J'–J''	Frequency (MHz)[a]	(kHz/Pa)	(kHz/Torr)
F_1–F_1	2_2^{1+}–1_2^{1-}	2 509 948.626 (44)	0.694 (64)	92.5 (85)
F_1–F_1	2_2^{1-}–1_2^{1+}	2 514 316.403 (28)	−0.068 (35)	−9.1 (46)
F_1–F_1	3_2^{1-}–2_2^{1+}	3 543 779.094 (39)	0.751 (68)	100.1 (91)
F_1–F_1	3_2^{1+}–2_2^{1-}	3 551 185.374 (11)	0.282 (18)	37.7 (24)
F_2–F_2	2_2^{1+}–1_2^{1-}	3 036 276.151 (32)	−0.146 (38)	−19.5 (51)
F_2–F_2	2_2^{1-}–1_2^{1+}	3 036 645.512 (19)	−0.269 (25)	−35.9 (33)
F_2–F_2	3_2^{1+}–2_2^{1-}	4 209 632.492 (108)	[c]	[c]

[a]Transition frequencies at zero pressure as calculated in the least squares fit, with 1σ uncertainties of the last digits in parentheses.
[b]Pressure shifts calculated assuming a linear relationship between pressure and transition frequency, with 1σ uncertainties of the last digits in parentheses.
[c]No statistically significant pressure shift was observed for this line.

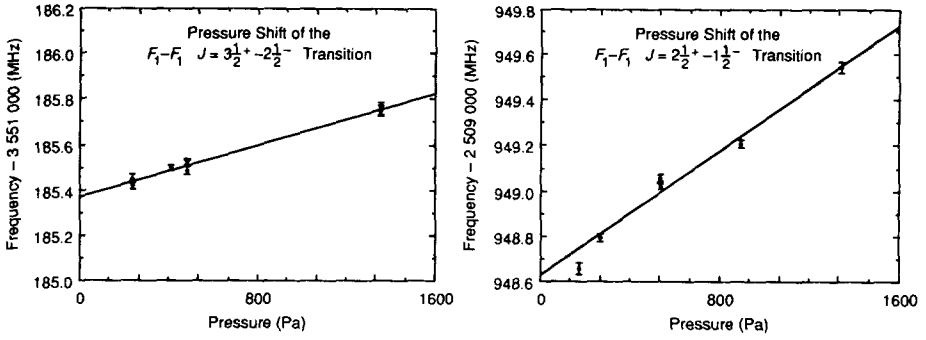

FIG. 3. Pressure shifts of two $v = 0$ transitions in OH, with helium as the buffer gas. Each data point is plotted with its 1σ error bars. The fitted pressure shifts are shown as solid lines (1600 Pa = 12 Torr).

$B\mathbf{R}^2 = B(\mathbf{J} - \mathbf{L} - \mathbf{S})^2$. Either representation is equally valid, of course, and will fit the experimental data similarly. However, the values of the fitted parameters are dependent on which formulation is used: the rotational constants are obviously affected, but so are any constants describing interactions for which centrifugal distortion terms are included. Brown *et al.* (*20*) have discussed the differences between these two formalisms and given interconversion formulas for the rotational, spin–orbit, and spin–rotation parameters. We have extended these formulas to include lambda-doubling and hyperfine parameters, as given in Table II. We required these formulas in order to convert Coxon's $\mathbf{R}^2$ parameters to $\mathbf{N}^2$ parameters for our least-squares fitting. Since our TuFIR data are not sensitive to all of the molecular parameters, we wanted to fix many of them at Coxon's values.

One point of possible confusion concerns the spin–rotation operator. The interconversion formulas given in Ref. (*20*) assume a spin–rotation operator of the form

TABLE II

Interconversion of Lambda-Doubling and Hyperfine Parameters Between the $\mathbf{N}^2$ and $\mathbf{R}^2$ Formalisms[a]

$\mathbf{N}^2$	$= f(\mathbf{R}^2)$	$\mathbf{R}^2$	$= f(\mathbf{N}^2)$
β	$= \beta^* - \Lambda^2\beta_D^* + \Lambda^4\beta_H^* - \Lambda^6\beta_L^*$	β^*	$= \beta + \Lambda^2\beta_D + \Lambda^4\beta_H + \Lambda^6\beta_L$
β_D	$= \beta_D^* - 2\Lambda^2\beta_H^* + 3\Lambda^4\beta_L^*$	β_D^*	$= \beta_D + 2\Lambda^2\beta_H + 3\Lambda^4\beta_L$
β_H	$= \beta_H^* - 3\Lambda^2\beta_L^*$	β_H^*	$= \beta_H + 3\Lambda^2\beta_L$
β_L	$= \beta_L^*$	β_L^*	$= \beta_L$
$\mathbf{N}^2$	$= f(\mathbf{R}^2)$[b]	$(\mathbf{R}^2)$[b]	$= f(\mathbf{N}^2)$
A	$= A^*$	A^*	$= A$
γ	$= \gamma^* - \Lambda^2\gamma_D^*$	γ^*	$= \gamma + \Lambda^2\gamma_D$
γ_D	$= \gamma_D^*$	γ_D^*	$= \gamma_D$

[a]The parameter β represents any of the lambda-doubling ($o, p, q, p + 2q, \ldots$) or hyperfine ($a, b, c, d, \ldots$) parameters; the absence or presence of an asterisk denotes parameters belonging to the $\mathbf{N}^2$ or $\mathbf{R}^2$ Hamiltonian, respectively.

[b]Coxon's $\mathbf{R}^2$ Hamiltonian (9), taken from Ref. (21), in which the spin–rotation operator is written as $\gamma\mathbf{N}\cdot\mathbf{S}$ instead of $\gamma\mathbf{R}\cdot\mathbf{S}$. The interconversion formulas for all other parameters in Coxon's Hamiltonian are the same as those given above and in Ref. (20).

$\gamma \mathbf{R} \cdot \mathbf{S}$ in the $\mathbf{R}^2$ formalism and $\gamma \mathbf{N} \cdot \mathbf{S}$ in the $\mathbf{N}^2$ formalism. Coxon, following earlier work by Brown *et al.* (*21*), used the form $\gamma \mathbf{N} \cdot \mathbf{S}$ in his $\mathbf{R}^2$ Hamiltonian. This choice alters the conversion formulas of Ref. (*20*) for the parameters A and γ, so we give interconversion formulas between Coxon's Hamiltonian and the $\mathbf{N}^2$ Hamiltonian for these two parameters in Table II as well. The matrix elements of the $\mathbf{N}^2$ Hamiltonian for a $^2\Pi$ state are given in Refs. (*22*) and (*23*).[2]

There is a well-known indeterminacy between the parameters describing the spin–rotation interaction (γ) and the centrifugal distortion correction to the spin–orbit interaction (A_D) in a $^2\Pi$ state (*24*). Since the spin–rotation interaction is expected to dominate in the OH $X\,^2\Pi$ state, we constrained A_D to be zero in our least-squares fitting. As a consequence, the parameters A, γ, and γ_D must be regarded as effective constants.

(D) Least-Squares Fitting of the Data

Using the effective Hamiltonian described above, we fitted by weighted least squares the observed transitions for the $v = 0$–3 levels of the OH $X\,^2\Pi$ state. Figure 1 displays an energy level diagram for the OH ground state, with notations for the transitions we observed. The observed and calculated transitions are given in Table III. Table IV lists microwave lambda-doubling transitions within the $v = 3$ level measured by other authors which we included in our data set, as discussed below. The results of least-squares fitting are presented in Table V. We discuss the fitting of each vibrational level in turn.

(i) $v = 0$. As noted earlier, Brown *et al.* (*10*) previously studied the OH $X\,^2\Pi$ ($v = 0$) level in our laboratory at NIST using TuFIR spectroscopy. Since that time, we have improved the experimental method in two significant ways (*12*). First, we now fit by least squares the lineshape of each spectrum using a computer; previously, transition line centers were estimated by eye from chart paper or with the aid of a computer display. Second, we now insert a length scrambler in the FIR radiation path in order to eliminate standing waves and thus flatten the spectrometer baseline.

The observed frequencies for $v = 0$ are given in Table III. We were unable to measure transition frequencies for any of the fine structure transitions of the $v = 0$ level over a sufficient pressure range to make an accurate extrapolation to zero pressure. These transitions, which are about 100× weaker than the pure rotational transitions (*25*), are very important, for they provide a direct measure of the spin–orbit splitting of the ground state. Therefore, we included data for these transitions (as well as for a pair of pure rotational transitions in the F_2 spin component) from the earlier TuFIR study of Brown *et al.* (*10*). We varied only B, D, A, γ, and γ_D in the least-squares fitting of the data. The lambda-doubling and proton hyperfine parameters were fixed at the values given by Brown *et al.* (*17*). The limited range of the data (three rotational intervals) also prevented us from determining the rotational centrifugal distortion constant H, so we constrained it to the value given in Ref. (*17*). Each datum was weighted by the square of the inverse of its experimental uncertainty. The variance of the fit relative to the experimental uncertainties (*26*) is 1.64. The calculated frequencies in this table form a definitive set for OH as is evidenced by the factor of five decrease in the values of O−C here, compared with those in Ref. (*10*).

[2] A. J. Merer has kindly pointed out a misprint in Table I of Ref. (*23*): The $\langle \frac{1}{2}, f/e, J-1 | H | \frac{3}{2}, e/f, J \rangle$ matrix element should read $\frac{1}{2} P(J) \{ b \mp eQq_2 T(J - \frac{1}{2}) \} [(2J+3)/(2J-1)]^{1/2}$.

TABLE III

Observed and Calculated Frequencies of Far-Infrared Transitions of the OH $X\,^2\Pi$ State (v = 0–3)

Transition				Frequency (MHz)		
v	F_i'–F_j''	J'–J''	F'–F''	Observed[a]	Calculated[b]	O–C
0	F_1–F_1	$2\frac{1}{2}$–$1\frac{1}{2}$	3^+–2^-	2 509 948.626 (44)	2 509 948.662 (30)	–0.036
			2^+–1^-		2 509 987.829 (30)	
			2^+–2^-		2 509 934.713 (30)	
			3^-–2^+	2 514 316.403 (28)	2 514 316.386 (30)	0.017
			2^-–1^+		2 514 353.165 (30)	
			2^-–2^+		2 514 298.092 (30)	
	F_1–F_1	$3\frac{1}{2}$–$2\frac{1}{2}$	4^-–3^+	3 543 779.094 (39)	3 543 779.072 (14)	0.022
			3^-–2^+		3 543 800.545 (14)	
			3^-–3^+		3 543 786.596 (14)	
			4^+–3^-	3 551 185.374 (11)	3 551 185.376 (14)	–0.002
			3^+–2^-		3 551 204.413 (14)	
			3^+–3^-		3 551 186.118 (14)	
	F_1–F_1	$4\frac{1}{2}$–$3\frac{1}{2}$	5^+–4^-		4 592 484.333 (77)	
			4^+–3^-		4 592 498.180 (77)	
			4^+–4^-		4 592 505.704 (77)	
			5^-–4^+		4 602 869.505 (77)	
			4^-–3^+		4 602 881.126 (77)	
			4^-–4^+		4 602 881.868 (77)	
	F_2–F_2	$1\frac{1}{2}$–$\frac{1}{2}$	2^-–1^+		1 834 746.874 (35)	
			1^-–0^+		1 834 749.951 (35)	
			1^-–1^+		1 834 735.017 (35)	
			2^+–1^-	1 837 816.390 (50)[c]	1 837 816.342 (35)	0.048
			1^+–0^-	1 837 836.520 (60)[c]	1 837 836.556 (35)	–0.036
			1^+–1^-		1 837 746.102 (35)	
	F_2–F_2	$2\frac{1}{2}$–$1\frac{1}{2}$	3^+–2^-	3 036 276.151 (32)	3 036 276.074 (20)	0.077
			2^+–1^-		3 036 270.093 (20)	
			2^+–2^-		3 036 258.236 (20)	
			3^-–2^+	3 036 645.512 (19)	3 036 645.544 (20)	–0.032
			2^-–1^+		3 036 644.222 (20)	
			2^-–2^+		3 036 573.983 (20)	
	F_2–F_2	$3\frac{1}{2}$–$2\frac{1}{2}$	4^-–3^+		4 212 298.573 (106)	
			3^-–2^+		4 212 292.784 (106)	
			3^-–3^+		4 212 274.946 (106)	
			4^+–3^-	4 209 632.492 (108)	4 209 632.448 (106)	0.044
			3^+–2^-		4 209 629.974 (106)	
			3^+–3^-		4 209 558.413 (106)	
	F_2–F_1	$\frac{1}{2}$–$1\frac{1}{2}$	1^+–2^-		3 786 131.875 (156)	
			0^+–1^-		3 786 170.057 (156)	
			1^+–1^-		3 786 184.991 (156)	
			1^-–2^+	3 789 214.99 (40)[c]	3 789 215.182 (156)	–0.19
			0^-–1^+	3 789 179.79 (27)[c]	3 789 179.802 (156)	–0.01
			1^-–1^+		3 789 270.255 (156)	
	F_2–F_1	$1\frac{1}{2}$–$2\frac{1}{2}$	2^-–3^+		3 110 930.087 (153)	
			1^-–2^+		3 110 932.179 (153)	
			2^-–2^+		3 110 944.036 (153)	
			2^+–3^-	3 112 715.01 (19)[c]	3 112 715.138 (153)	–0.13
			1^+–2^-	3 112 663.41 (21)[c]	3 112 663.192 (153)	0.22
			2^+–2^-		3 112 733.432 (153)	

[a]Observed frequencies are from the present work and were measured using third order TuFIR, except where noted. The numbers in parentheses are the estimated 1σ uncertainties in units of the last quoted digits.
[b]Calculated frequencies were obtained using the molecular parameters given in Table V. The numbers in parentheses are the estimated 1σ uncertainties in units of the last quoted digits, obtained from the least squares fit.
[c]From TuFIR study of Brown *et al.* (10).
[d]Measured using second order TuFIR.
[e]From LMR study of Davies *et al.* (27).

structure transition. We determined five parameters in the least-squares fitting: B, D, A, γ, and γ_D. The centrifugal distortion parameter H and the lambda-doubling and hyperfine parameters were fixed at the values determined by Coxon in his global fit (9), after conversion to our N^2 Hamiltonian. The relative variance of the least-squares fit is 0.99.

(iii) $v = 2$. We measured five rotational intervals in the $v = 2$ level of OH; efforts at detecting a fine structure transition were unsuccessful. However, Davies *et al.* (27)

TABLE III—*Continued*

Transition				Frequency (MHz)		
v	$F_i'-F_i''$	$J'-J''$	$F'-F''$	Observed[a]	Calculated[b]	O − C
1	F_1-F_1	$2\frac{1}{2}-1\frac{1}{2}$	3^+-2^-	2 420 297.49 (20)	2 420 297.46 (12)	0.04
			2^+-1^-		2 420 334.20 (12)	
			2^+-2^-		2 420 286.69 (12)	
			3^--2^+	2 424 357.02 (20)	2 424 356.96 (12)	0.06
			2^--1^+		2 424 391.53 (12)	
			2^--2^+		2 424 342.27 (12)	
	F_1-F_1	$3\frac{1}{2}-2\frac{1}{2}$	4^--3^+	3 414 759.08 (20)	3 414 759.41 (11)	−0.33
			3^--2^+		3 414 779.81 (11)	
			3^--3^+		3 414 769.05 (11)	
			4^+-3^-	3 421 691.67 (20)	3 421 691.46 (11)	0.21
			3^+-2^-		3 421 709.62 (11)	
			3^+-3^-		3 421 694.92 (11)	
	F_1-F_1	$4\frac{1}{2}-3\frac{1}{2}$	5^+-4^-	4 422 678.47 (50)	4 422 678.17 (29)	0.30
			4^+-3^-		4 422 691.47 (29)	
			4^+-4^-		4 422 701.11 (29)	
			5^--4^+	4 432 452.95 (50)	4 432 452.97 (29)	−0.03
			4^--3^+		4 432 464.19 (29)	
			4^--4^+		4 432 467.65 (29)	
	F_2-F_2	$1\frac{1}{2}-\frac{1}{2}$	2^--1^+	1 759 368.12 (20)	1 759 368.01 (12)	0.11
			1^--0^+		1 759 371.91 (12)	
			1^--1^+		1 759 355.29 (12)	
			2^+-1^-		1 762 353.44 (12)	
			1^+-0^-		1 762 373.51 (12)	
			1^+-1^-		1 762 285.19 (12)	
	F_2-F_2	$2\frac{1}{2}-1\frac{1}{2}$	3^+-2^-	2 913 055.62 (20)	2 913 055.87 (11)	−0.25
			2^+-1^-		2 913 050.12 (11)	
			2^+-2^-		2 913 037.40 (11)	
			3^--2^+	2 913 520.79 (20)	2 913 520.64 (11)	0.14
			2^--1^+		2 913 519.23 (11)	
			2^--2^+		2 913 450.98 (11)	
	F_2-F_2	$3\frac{1}{2}-2\frac{1}{2}$	4^--3^+	4 043 449.29 (20)	4 043 449.36 (14)	−0.07
			3^--2^+		4 043 443.61 (14)	
			3^--3^+		4 043 425.13 (14)	
			4^+-3^-	4 041 044.18 (20)	4 041 044.09 (14)	0.09
			3^+-2^-		4 041 041.42 (14)	
			3^+-3^-		4 040 971.76 (14)	
	F_2-F_1	$1\frac{1}{2}-2\frac{1}{2}$	2^--3^+		3 142 965.82 (50)	
			1^--2^+		3 142 963.86 (50)	
			2^--2^+		3 142 976.58 (50)	
			2^+-3^-	3 144 890.41 (50)[d]	3 144 890.41 (50)	0.00
			1^+-2^-		3 144 836.86 (50)	
			2^+-2^-		3 144 905.11 (50)	
2	F_1-F_1	$2\frac{1}{2}-1\frac{1}{2}$	3^+-2^-	2 331 523.25 (20)	2 331 523.13 (9)	0.12
			2^+-1^-		2 331 557.43 (9)	
			2^+-2^-		2 331 515.96 (9)	
			3^--2^+	2 335 280.92 (20)	2 335 280.97 (9)	−0.05
			2^--1^+		2 335 313.30 (9)	
			2^--2^+		2 335 270.25 (9)	
	F_1-F_1	$3\frac{1}{2}-2\frac{1}{2}$	4^--3^+	3 287 211.97 (20)	3 287 212.23 (8)	−0.26
			3^--2^+		3 287 231.57 (8)	
			3^--3^+		3 287 224.40 (8)	
			4^+-3^-	3 293 674.59 (20)	3 293 674.42 (8)	0.16
			3^+-2^-		3 293 691.70 (8)	
			3^+-3^-		3 293 680.98 (8)	
	F_1-F_1	$4\frac{1}{2}-3\frac{1}{2}$	5^+-4^-	4 254 971.45 (50)	4 254 971.16 (21)	0.28
			4^+-3^-		4 254 983.92 (21)	
			4^+-4^-		4 254 996.09 (21)	
			5^--4^+	4 264 135.85 (50)	4 264 135.91 (21)	−0.06
			4^--3^+		4 264 146.73 (21)	
			4^--4^+		4 264 153.29 (21)	
	F_2-F_2	$1\frac{1}{2}-\frac{1}{2}$	2^--1^+		1 685 296.18 (12)	
			1^--0^+		1 685 300.94 (12)	
			1^--1^+		1 685 282.34 (12)	
			2^+-1^-		1 688 189.01 (12)	
			1^+-0^-		1 688 209.02 (12)	
			1^+-1^-		1 688 122.43 (12)	

TABLE III—*Continued*

Transition				Frequency (MHz)		
v	F_i'–F_i''	J'–J''	F'–F''	Observed[a]	Calculated[b]	O – C
2	F_2–F_2	$2\frac{1}{2}$–$1\frac{1}{2}$	3^+–2^-	2 791 794.15 (20)	2 791 794.18 (10)	–0.03
			2^+–1^-		2 791 788.63 (10)	
			2^+–2^-		2 791 774.79 (10)	
			3^-–2^+	2 792 343.62 (20)	2 792 343.58 (10)	0.04
			2^-–1^+		2 792 342.05 (10)	
			2^-–2^+		2 792 275.48 (10)	
	F_2–F_2	$3\frac{1}{2}$–$2\frac{1}{2}$	4^-–3^+	3 877 076.24 (20)	3 877 076.14 (10)	0.10
			3^-–2^+		3 877 070.40 (10)	
			3^-–3^+		3 877 051.02 (10)	
			4^+–3^-	3 874 923.19 (20)	3 874 923.29 (10)	–0.10
			3^+–2^-		3 874 920.42 (10)	
			3^+–3^-		3 874 852.32 (10)	
	F_2–F_1	$\frac{1}{2}$–$1\frac{1}{2}$	1^+–2^-	3 821 773. (30)[c]	3 821 768. (16)	5.80
			0^+–1^-		3 821 790. (16)	
			1^+–1^-		3 821 809. (16)	
			1^-–2^+	3 824 668. (30)[c]	3 824 673. (16)	–5.18
			0^-–1^+		3 824 629. (16)	
			1^-–1^+		3 824 716. (16)	
3	F_1–F_1	$2\frac{1}{2}$–$1\frac{1}{2}$	3^+–2^-		2 243 276.99 (36)	
			2^+–1^-		2 243 308.83 (36)	
			2^+–2^-		2 243 273.76 (36)	
			3^-–2^+		2 246 738.56 (36)	
			2^-–1^+		2 246 768.62 (36)	
			2^-–2^+		2 246 732.14 (36)	
	F_1–F_1	$3\frac{1}{2}$–$2\frac{1}{2}$	4^-–3^+		3 160 634.33 (35)	
			3^-–2^+		3 160 652.61 (35)	
			3^-–3^+		3 160 649.39 (35)	
			4^+–3^-		3 166 629.28 (35)	
			3^+–2^-		3 166 645.67 (35)	
			3^+–3^-		3 166 639.25 (35)	
	F_1–F_1	$4\frac{1}{2}$–$3\frac{1}{2}$	5^+–4^-	4 088 705.20 (50)	4 088 705.20 (29)	–0.01
			4^+–3^-		4 088 717.43 (29)	
			4^+–4^-		4 088 732.48 (29)	
			5^-–4^+	4 097 257.67 (50)	4 097 257.66 (29)	0.01
			4^-–3^+		4 097 268.10 (29)	
			4^-–4^+		4 097 278.08 (29)	
	F_2–F_2	$1\frac{1}{2}$–$\frac{1}{2}$	2^-–1^+		1 612 259.97 (15)	
			1^-–0^+		1 612 265.67 (15)	
			1^-–1^+		1 612 244.80 (15)	
			2^+–1^-		1 615 049.03 (15)	
			1^+–0^-		1 615 069.08 (15)	
			1^+–1^-		1 614 983.84 (15)	
	F_2–F_2	$2\frac{1}{2}$–$1\frac{1}{2}$	3^+–2^-	2 672 052.01 (20)	2 672 051.94 (14)	0.07
			2^+–1^-		2 672 046.57 (14)	
			2^+–2^-		2 672 031.40 (14)	
			3^-–2^+	2 672 673.07 (20)	2 672 673.14 (14)	–0.07
			2^-–1^+		2 672 671.51 (14)	
			2^-–2^+		2 672 606.32 (14)	
	F_2–F_2	$3\frac{1}{2}$–$2\frac{1}{2}$	4^-–3^+	3 712 574.42 (20)	3 712 574.49 (14)	–0.07
			3^-–2^+		3 712 568.73 (14)	
			3^-–3^+		3 712 548.19 (14)	
			4^+–3^-	3 710 664.04 (20)	3 710 663.97 (14)	0.07
			3^+–2^-		3 710 660.87 (14)	
			3^+–3^-		3 710 594.05 (14)	
	F_2–F_1	$\frac{1}{2}$–$1\frac{1}{2}$	1^+–2^-	3 839 464. (30)[c]	3 839 466. (18)	–1.58
			0^+–1^-		3 839 480. (18)	
			1^+–1^-		3 839 501. (18)	
			1^-–2^+	3 842 268. (30)[c]	3 842 267. (18)	0.97
			0^-–1^+		3 842 218. (18)	
			1^-–1^+		3 842 303. (18)	

have measured the F_2–F_1, $J = \frac{1}{2}$–$1\frac{1}{2}$ fine structure transition for both parities of the $v = 0$–3 levels by LMR. These authors give 60 MHz as a "conservative upper limit" to their uncertainty, arising principally from the lack of an absolute calibration of their magnet. In comparing their measured fine structure splittings of the $v = 0$ and

TABLE IV

OH $X^2\Pi$ (v = 3) Microwave Lambda-Doubling Transitions (Observed by Other Workers) Which Were Included in the Data Set

Transition			Frequency (MHz)			
F_i	J	F'–F''	Observed[a]	Calculated[b]	O – C	Reference
F_1	$1\frac{1}{2}$	1^+–1^-	1 292.27 (20)	1 292.59 (2)	–0.32	(28, 29)[c]
		2^+–2^-	1 293.68 (20)	1 294.00 (2)	–0.32	(28, 29)[c]
	$3\frac{1}{2}$	3^+–3^-	10 745.50 (30)	10 745.44 (14)	0.06	(30)
		4^+–4^-	10 750.50 (30)	10 750.52 (14)	–0.02	(30)
	$4\frac{1}{2}$	4^-–4^+	19 296.40 (60)	19 296.11 (19)	0.29	(30)
		5^-–5^+	19 303.20 (60)	19 302.98 (19)	0.22	(30)
	$6\frac{1}{2}$	6^-–6^+	43 511.93 (50)	43 511.93 (29)	0.00	(30)
		7^-–7^+	43 521.72 (50)	43 521.75 (29)	–0.03	(30)

[a]The numbers in parentheses are the estimated 1σ uncertainties in units of the last quoted digits.
[b]The numbers in parentheses are the calculated 1σ uncertainties in units of the last quoted digits, obtained from the least squares fit.
[c]The average value from these two epr studies was used. The $F = 2$ and 1 hyperfine components of this blended epr line were deconvoluted using a 3:5 hyperfine-weighted splitting. In Ref. (30) a 1:1 hyperfine-weighted splitting was used for this line.

1 levels (averaged for the two parities) with our higher resolution data, we find discrepancies of 28 and 8 MHz, respectively. By comparison, Coxon's fine structure splittings (*9*), which are based on a merged fit to optical and infrared data, disagree with ours by 107 and 151 MHz for v = 0 and 1, respectively. These comparisons suggest that including the fine structure splittings of Davies *et al.* for the v = 2 and 3

TABLE V

Molecular Parameters of the OH $X^2\Pi$ State (v = 0–3)

	Value (MHz)[a]			
Parameter	$v = 0$	$v = 1$	$v = 2$	$v = 3$
B	555 661.525 (14)	534 347.446 (36)	513 318.394 (34)	492 495.787 (70)
D	57.228 51 (67)	56.068 1 (14)	55.026 6 (12)	54.129 1 (21)
H	[0.004 236]	[0.004 060 37]	[0.003 847 71]	[0.003 596 54]
A	–4 168 640.95 (24)	–4 176 724.49 (81)	–4 184 747. (14)	–4 192 390. (16)
γ	–3 573.22 (13)	–3 410.22 (42)	–3 247.0 (16)	–3 072.5 (13)
γ_D	0.687 6 (62)	0.679 (16)	0.693 (16)	[0.739 6]
p	[7 053.098 46]	[6 735.686 4]	[6 413.370 8]	6 082.27 (16)
p_D	[–1.550 962]	[–1.548 08]	[–1.545 08]	[–1.542 08]
$10^4 p_H$	[1.647]	[1.669]	[1.669]	[1.669]
q	[–1 159.991 650]	[–1 107.429 6]	[–1 054.527 9]	–1 000.905 (22)
q_D	[0.442 032 0]	[0.434 112 0]	[0.427 386 1]	0.419 72 (62)
$10^5 q_H$	[–8.237]	[–8.355 1]	[–8.355 1]	[–8.355 1]
a	[86.111 6]	[82.073]	[78.130]	[74.283]
b_F	[–73.253 7]	[–77.101]	[–81.938]	[–87.677]
c	[130.641]	[125.330]	[120.175]	[115.186]
d	[56.683 8]	[53.820 8]	[51.036 6]	[48.326 7]
d_D	[–0.022 76]	[–0.022 85]	[–0.022 85]	[–0.022 84]
C_l	[–0.099 71]	[–0.097 84]	[–0.096 24]	[–0.094 58]
C_l'	[0.006 43]	[0.006 49]	[0.006 49]	[0.006 51]
f[b]	8	7	7	9
Variance[c]	1.64	0.99	0.54	0.69

[a]Values in parentheses are the calculated 1σ errors in units of the last quoted digits. Parameters enclosed by square brackets were constrained at those values. The constrained values were taken from Ref. (10) for v = 0 and from Ref. (9) for v = 1–3, with the latter converted to N^2 values as described in the text.
[b]f = Degrees of freedom = (Number of data points – Number of varied parameters).
[c]Variance relative to the experimental errors (26).

levels in our data set is preferable to simply fixing the values of the $v = 2$ and 3 spin–orbit constants to those given by Coxon. The fine structure splittings reported by Davies *et al.* are averages over the hyperfine splittings; therefore, we calculated the position of the strongest hyperfine component of each fine structure transition using our constrained hyperfine parameters and added these transitions to our data sets for the $v = 2$ and 3 levels. We estimate the uncertainties in these frequencies as 30 MHz, as it appears that 60 MHz is too pessimistic.

We determined the five parameters B, D, A, γ, and γ_D in the least-squares fit. All other parameters were fixed at Coxon's values (*9*). The relative variance of the fit is 0.54.

(iv) $v = 3$. Our data for the $v = 3$ level include one rotational transition in the F_1 spin component and two transitions in the F_2 component, each measured for both parity components. As described above, we also included the fine structure transitions of Davies *et al.* (*27*) in our data set. However, microwave lambda-doubling transitions in the $v = 3$ level have been observed only within the F_1 spin component (*28–30*); the lambda-doubling of the F_2 component is thus poorly determined from optical and infrared data (*9*). Therefore, we included the available microwave data in our least-squares fit (see Table IV) and determined accurate values for the p, q, and q_D lambda-doubling parameters, as well as for B, D, A, and γ. The microwave data were weighted using experimental uncertainties estimated by Coxon *et al.* (*30*). The relative variance of the least-squares fit is 0.69.

4. DISCUSSION

The molecular constants and transition frequencies reported in this work for the $v = 1$–3 levels are considerably more accurate than those reported previously. The uncertainty of the spin–orbit parameter A is about 250 times smaller than that reported by Coxon (*9*) for the $v = 1$ level and about 30 times smaller for the $v = 2$ and 3 levels. The uncertainties of the B, D, and γ molecular constants in the $v = 1$–3 levels are about 20 times smaller than Coxon's.[3] These significant improvements result from the much higher resolution of TuFIR spectroscopy in comparison with infrared and optical spectroscopy, upon which Coxon's values are based. Coxon's values for the $v = 1$–3 parameters are in agreement with ours at the 3σ level, with the exception of the p and q lambda-doubling parameters in the $v = 3$ level, which are just outside agreement at 3σ.

The improvement in the $v = 0$ molecular constants is less dramatic because the $v = 0$ level had already been studied by TuFIR spectroscopy (*10*). However, in this work we measured one additional rotational interval in the F_2 spin component, and the recent improvements in the TuFIR experimental technique have increased the accuracy of the experimental transition frequencies. The parameters determined in Ref. (*10*) agree with ours within experimental error.

ACKNOWLEDGMENTS

This work was supported in part by NASA Contract W-15,047. The authors thank Lyndon Zink for helpful advice and experimental assistance and John Brown for profitable discussions regarding the Stark shifts and the least-squares fitting.

RECEIVED: June 10, 1992

[3] In Ref. (9), Coxon used a Dunham-type expansion for the A, D, and γ molecular constants. We calculated the uncertainties in the v-specific constants by expanding the estimated errors in the Dunham coefficients. This process neglects the correlations between the errors in the coefficients, but presumably gives approximate uncertainties for the v-specific molecular constants.

REFERENCES

1. M. NICOLET, *Rev. Geophys. Space Phys.* **13,** 593–636 (1975).
2. R. ATKINSON AND A. C. LLOYD, *J. Phys. Chem. Ref. Data* **13,** 315–444 (1984).
3. J. A. MILLER AND G. A. FISK, *Chem. Eng. News* **65**(35), 22–46 (1987).
4. S. WEINREB, A. H. BARRETT, M. L. MEEKS, AND J. C. HENRY, *Nature* **200,** 829 (1963).
5. J. W. V. STOREY, D. M. WATSON, AND C. H. TOWNES, *Astrophys. J.* **244,** L27–L30 (1981).
6. P. KRISTIANSEN AND L. VESETH, *J. Chem. Phys.* **84,** 2711–2719 (1986).
7. P. KRISTIANSEN AND L. VESETH, *J. Chem. Phys.* **84,** 6336–6344 (1986).
8. D. P. CHONG, S. R. LANGHOFF, AND C. W. BAUSCHLICHER, JR., *J. Chem. Phys.* **94,** 3700–3706 (1991).
9. J. A. COXON, *Can. J. Phys.* **58,** 933–949 (1980). See also J. A. Coxon and S. C. Foster, *Can. J. Phys.* **60,** 41–48 (1982) and J. A. Coxon, A. D. Sappey, and R. A. Copeland, *J. Mol. Spectrosc.* **145,** 41–55 (1991).
10. J. M. BROWN, L. R. ZINK, D. A. JENNINGS, K. M. EVENSON, A. HINZ, AND I. G. NOLT, *Astrophys. J.* **307,** 410–413 (1986).
11. I. G. NOLT, J. V. RADOSTITZ, G. DILONARDO, K. M. EVENSON, D. A. JENNINGS, K. R. LEOPOLD, M. D. VANEK, L. R. ZINK, A. HINZ, AND K. V. CHANCE, *J. Mol. Spectrosc.* **125,** 274–287 (1987).
12. T. D. VARBERG AND K. M. EVENSON, *Astrophys. J.* **385,** 763–765 (1992).
13. F. R. PETERSEN, E. C. BEATY, AND C. R. POLLOCK, *J. Mol. Spectrosc.* **102,** 112–122 (1983).
14. L. R. ZINK, K. M. EVENSON, F. MATSUSHIMA, T. NELIS, AND R. L. ROBINSON, *Astrophys. J.* **371,** L85–L86 (1991).
15. K. V. CHANCE, D. A. JENNINGS, K. M. EVENSON, M. D. VANEK, I. G. NOLT, J. V. RADOSTITZ, AND K. PARK, *J. Mol. Spectrosc.* **146,** 375–380 (1991).
16. W. GORDY AND R. L. COOK, "Microwave Molecular Spectra," Eq. (15.139), p. 832, Wiley-Interscience, New York, 1984.
17. J. M. BROWN, C. M. L. KERR, F. D. WAYNE, K. M. EVENSON, AND H. E. RADFORD, *J. Mol. Spectrosc.* **86,** 544–554 (1981).
18. W. GORDY AND R. L. COOK, "Microwave Molecular Spectra," Eq. (10.3), p. 452, Wiley-Interscience, New York, 1984.
19. J. M. BROWN, E. A. COLBOURN, J. K. G. WATSON, AND F. D. WAYNE, *J. Mol. Spectrosc.* **74,** 294–318 (1979).
20. J. M. BROWN, A. S.-C. CHEUNG, AND A. J. MERER, *J. Mol. Spectrosc.* **124,** 464–475 (1987).
21. J. M. BROWN, M. KAISE, C. M. L. KERR, AND D. J. MILTON, *Mol. Phys.* **36,** 553–582 (1978).
22. C. AMIOT, J.-P. MAILLARD, AND J. CHAUVILLE, *J. Mol. Spectrosc.* **87,** 196–218 (1981).
23. M. C. L. GERRY, A. J. MERER, U. SASSENBERG, AND T. C. STEIMLE, *J. Chem. Phys.* **86,** 4754–4761 (1987).
24. J. M. BROWN AND J. K. G. WATSON, *J. Mol. Spectrosc.* **65,** 65–74 (1977).
25. J. M. BROWN, J. E. SCHUBERT, K. M. EVENSON, AND H. E. RADFORD, *Astrophys. J.* **258,** 899–903 (1982).
26. D. L. ALBRITTON, A. L. SCHMELTEKOPF, AND R. N. ZARE, *in* "Molecular Spectroscopy: Modern Research" (K. N. Rao, Ed.), Vol. 2, p. 1, Academic Press, New York, 1976.
27. P. B. DAVIES, W. HACK, A. W. PREUSS, AND F. TEMPS, *Chem. Phys. Lett.* **64,** 94–97 (1979).
28. P. N. CLOUGH, A. H. CURRAN, AND B. A. THRUSH, *Proc. R. Soc. London, Ser. A.* **323,** 541–554 (1971).
29. K. P. LEE, W. G. TAM, R. LAROUCHE, AND G. A. WOONTON, *Can. J. Phys.* **49,** 2207–2214 (1971).
30. J. A. COXON, K. V. L. N. SASTRY, J. A. AUSTIN, AND D. H. LEVY, *Can. J. Phys.* **57,** 619–634 (1979).